Jilin Daxue Xuebao (Gongxueban)/Journal of Jilin University (Engineering and Technology Edition)
ISSN：1671-5497
E-Publication Online Open Access
Vol: 41 Issue: 12-2022
DOI 10.17605/OSF.IO/MVWDU

A ROBUST AND SCALE INVARIANT METHOD FOR IMAGE FORGERY CLASSIFICATION USING EDGE WEIGHTED LOCAL TEXTURE FEATURES

ARSLAN AKRAM
Ph.D. Scholar, Department of Computer Science, Superior University Lahore, Lahore, Pakistan.
Email: aaadoula11@gmail.com

Dr. ARFAN JAFFAR
PhD, Professor Department of Computer Science and Information Technology, Superior University Lahore, Lahore, Pakistan. Email: arfan.jaffar@superior.edu.pk

Dr. WASEEM IQBAL
PhD, Associate Professor Department of Software Engineering, Superior University Lahore, Lahore, Pakistan. Email: Waseem.iqbal@superior.edu.pk

M. SALMAN ALI
Mphil Scholar, Department of Computer Science, Superior University Lahore, Lahore, Pakistan.
Email: msalmanali0683@gmail.com

M. USMAN TARIQ
Mphil Scholar, Department of Computer Science, Superior University Lahore, Lahore, Pakistan.
Email: Tariqusman263@gmail.com

GHULAM ALI
Faculty of Computing, Department of Software Engineering, University of Okara, Okara, Pakistan.
Email: ghulamali@uo.edu.pk

Abstract

It has become easier to change the content of computerized photos as mixed media innovation has advanced. This is due to the wide availability of picture editing apps. If altered for a negative motive, created images can cause major social and legal problems. The detection of picture fraud requires the advancement of contemporary methods that can effectively spot modifications in sophisticated images. In photographs, joining mimicry is frequently used to hide the truth. Grafting creates sharp distinctions in the edges, corners, and smooth areas. Using picture grafting, discrete wavelet change, and histograms of discriminative vigorous neighborhood double designs, we proposed a novel method for finding picture imitations. A given color image is first converted to “YCbCr”, and the Cr and Cb components of the computerized image are then linked to DWT. DRLBP is used to show surface variation in each DWT subband. The final highlight trajectory is created by concatenating the DRLBP from every sub-band. After all, an SVM is used to produce an image fraud recognition demonstration. On openly available benchmark datasets, the suggested strategy's application and generalizability were evaluated. With 98.95% location accuracy, the suggested method outperformed cutting-edge imitation location techniques.

Keywords: Image forgery; splicing detection; DWT; DRLBP; SVM, Scale Invariant, Rotation Invariant, Machine Learning Approach, Image Forensic Analysis.

Jilin Daxue Xuebao (Gongxueban)/Journal of Jilin University (Engineering and Technology Edition)
ISSN：1671-5497
E-Publication Online Open Access
Vol: 41 Issue: 12-2022
DOI 10.17605/OSF.IO/MVWDU

1. INTRODUCTION

Numerous facets of society, like the Internet, print media, the defense industry, and surveillance security, among others, call on advanced photography. Since the content of an image may be changed with the aid of contemporary picture-changing instruments, photo confirmation may be a significant problem. Due to photo manipulation, society is dealing with problems like false advertising, extortion, falsification, dark mailing, etc. It is necessary to verify images before using them as a source of information or to support real-world claims. The majority of the time, especially with malicious intent, picture imitation is done via copy-move and splicing techniques. Through fraud preparation, images can be adjusted using similar image content or by merging the content of various images. If the altering strategy involves copying and pasting image content into the image, this fraud is referred to as copy-move; alternatively, it is stated as joining. Different kinds of post-processing (PP) operations are connected to the manufactured locations to stow away the imitation cues, including scaling, obscuring, commotion, compression, and turning.

The legal review of images began in 2000 [1]. Based on the grafting discovery component, several algorithms [2–6] were developed to detect grafting fraud and may be characterized as dynamic and detached (or dazzle) [1]. Dynamic strategies remove this watermark or signature with the first to confirm its realness. Dynamic approaches act on the idea that a provided image includes data like an imprint or sign at the moment of purchase to guarantee its validity. Due to the lack of data around the watermark or signature in the majority of circumstances, the use of these tactics is severely restricted. This constraint leads to the development of non-data-dependent inactive approaches for grafting fraud detection. In picture joining, the content of one picture is changed by copying and adhering to the content of another picture. A crucial and well-liked photo fraud tactic is joining. Picture joining location has developed into a crucial investigative area for computerized image fraud locations to maintain public confidence in computerized picture verification. The process of image grafting worsens

Figure 1: Original Image (Left) Spliced Image (right)

The uniformity, smoothness, and consistency of the material. These factors are quite important in identifying the fraudulent locations in the image. Modern picture grafting techniques take into account the many global factual aspects that are exhibited by unexpected irregularity in grafted images [4–7]. Figure 1 shows a case of grafted picture imitation.

Jilin Daxue Xuebao (Gongxueban)/Journal of Jilin University (Engineering and Technology Edition)
ISSN：1671-5497
E-Publication Online Open Access
Vol: 41 Issue: 12-2022
DOI 10.17605/OSF.IO/MVWDU

A given picture is first separated into sub-bands using DWT to identify the discontinuities in the picture caused by joining. The DWT's strong de-correlation ability talks to the coefficients of four wavelet sub-bands on an equal footing. We suggested a straightforward method using the DWT sub-band coefficients to grade the discontinuities introduced by grafting in images. Additionally, we suggest using a strict coding method that encodes the coefficients of the DWT sub-bands. We present a previously unexplored method to expose grafting fraud by segmenting chroma modules of a sample image operating DWT [22] keen on sub-bands for determining nearby gaps. This method is based on the future plot that measures gaps and their encrypting. We linked DRLBP [23] for coding to determine the neighborhood discontinuities. The DWT-DRLBP descriptor, which talks to a picture and is used for recognizing joining fraud, is what we refer to as the descriptor based on these tactics. Last but not least, SVM is used to spot picture imitation in modern images.

2. LITERATURE REVIEW

The majority of blind/passive joining fraud location tactics exist[5]. DCT coefficients, least, and most extreme channels were used by Alhamadi et al. [7] and Hwang et al. [8] to extract highlights from image squares and detect grafting fraud. Numerous computations make use of multi-resolution techniques like DWT [3, 9]. As an alternative to piece coordinating, filter highlights are used to spot grafting fraud [10]. The majority of joining imitation finding techniques are evaluated using the datasets from the Columbia Color (CC) DVMM [11], CASIA (v1.0) [12], and CASIA (v2.0)[12]. To differentiate joining fraud, Ng et al [13].’s offered a picture grafting discovery strategy constructed on 3D minutes of image range, although [14] transmitted highlights established on-camera reaction work to SVM. Shi et al [15].’s method for determining the position of an image graft applied 2D and 1D minutes, Markov chain probabilities (MCP), and DCT coefficients. The calculation's detailed exactness is 84.86% and it was assessed using the CASIA (v2.0) dataset. By combining Markov chain minutes, DCT, and DWT coefficients with SVM, He et al., [3] improved the precision to 89.76% of the Shi et al., method. For picture joining discovery, Markov probabilities (MP) were mined from the Cb channel in [16]. When tested on a sample of the CASIA (v2.0) datasets and the Columbia Color (CC) DVMM datasets, the computation achieved 89.24% and 95.49% accuracy, correspondingly. Zaho et al. [17] improved Wang et al. [16]'s implementation by outlining a chrominance channel to differentiate grafting mimicry.

With the modern advancements in UB (ubiquitous computing) and advanced channels, particularly computerized images, the identification of picture impersonation has emerged as the most important task for the safe and genuine transfer of mixed media content. Alahmad et al. (19) used DCT and LBP features to determine where to place photo grafts. Markov highlights were extracted by Pham et al. [20] to distinguish anomalies in images caused by grafting. SVM (Support Vector Machine) was used to classify data. Fragmentary entropy was extracted from DWT coefficients by Jalab et al. [21] and SVM was used for classification. Skillet [3] came up with a useful technique for

Jilin Daxue Xuebao (Gongxueban)/Journal of Jilin University (Engineering and Technology Edition)
ISSN：1671-5497
E-Publication Online Open Access
Vol: 41 Issue: 12-2022
DOI 10.17605/OSF.IO/MVWDU

locating copied locations in a photo frame. The suggested technique finds the indistinguishably altered locations by using geometric changes to identify the key points. A two-level keypoint detection approach was also developed by Emam et al. [4] to emphasize the picture-altering effects in smooth environments. To identify key point highlights from smooth districts, the scale-invariant highlight administrator and Harris corner finder were initially coupled. Finally, a multi-back locale arranges descriptor's slope histogram was constructed to accurately differentiate the several districts in a produced image. A novel fraud identification process based on the least and most extreme channels was developed by Hwang et al. [8]. The pixel-smart least and biggest differences between actual and fashioned photos are highlighted by the combination of least channel and most extreme channel. The execution of the fraud location process in composite localities advanced thanks to the analysis of introduction and non-interpolation. Recently, Wang et al. [9] developed a brand-new method for profound learning to determine where to place image grafts. The weighted mixture of three different types of highlighted extraction strategies is learned through the proposed convolutional neural network (CNN). The best set of parameters for highlight extraction techniques is learned using convolutional neural networks (CNNs).

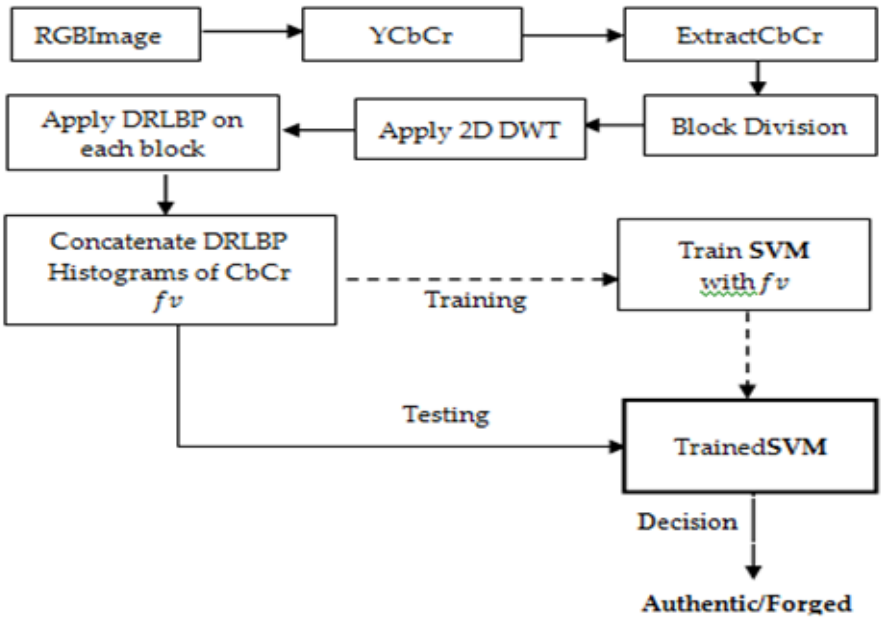

Figure 2: Intended Splicing Image Forgery Detection Methodology

Figure 2 shows how the test image has been rehabilitated to the YCbCr color area, where Cb, Cr, and Y are the luminance and chroma components, respectively. The luminance channel, which can hide the effects of material alteration, represents the content of the picture. Grafting alters the surface patterns, for example, lines, edges, and corners, that signify abrupt shifts. Chroma components make it simple to identify these imperfections in a picture's surface since they represent weak signals (corners,

Jilin Daxue Xuebao (Gongxueban)/Journal of Jilin University (Engineering and Technology Edition)
ISSN：1671-5497
E-Publication Online Open Access
Vol: 41 Issue: 12-2022
DOI 10.17605/OSF.IO/MVWDU

lines, and edges) [5, 16, 17]. Since the alterations caused by grafting are displayed in tall recurrent wavelet groups, grafting exposes the gaps in the way of the edges in pictures that influence the local composition of linked pictures and are well revealed using DWT factors. To examine these changes, we suggest the DWT-DRLBP descriptor, which first uses the Discrete Wavelet Transform (DWT) to break down the chroma components (CC) of a presented image into sub-bands and then converts these sub-bands using the DRLBP surface signifier, which may be a powerful surface descriptor. SVM receives the DWT-DRLBP descriptor of an image and decides if it is true or not. To determine whether a test image was fake or real, we linked an SVM with a two-lesson classifier [24]. Although the back vector machine VM is a direct classifier. The tests of the photo fraud dataset used in this study are not evenly divvied. An associated component trap is used to solve this problem. The tests were run using the LIBSVM portion given in [25].

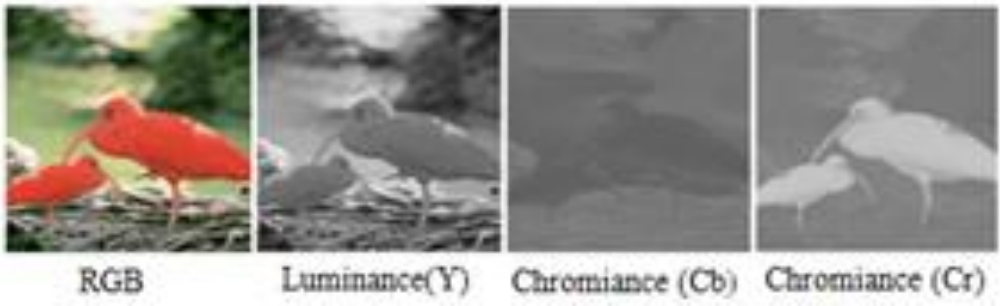

Figure 3: Y, Cb, and Cr components of an RGB image

3. METHODOLOGY

The test image disintegrated into four recurrence groups (LL, LH, HL, and HH) after discrete wavelet modification. The chroma components that make up these recurrence groups draw attention to the local abnormalities in the fashioned. The suggested image-joining algorithms combine DRLBP highlights with DWT-based chroma components. Due to this, a one-level DWT was first linked within the image, and later a DRLBP description was attached to emphasize the effects of the joining.

3.1. Wavelet Disintegration of Chroma Component

The DWT provides an exclusive and unfair image to efficiently assess the image surface with extreme resolution and minimal wavelet factors. In image grafting, the wavelet factors effectively draw attention to the fundamental variations. The tall differentiation that results from picture joining is given by the moo recurrence coefficients. The test image is carefully addressed using the moo recurrence features. The method of picture representation becomes very simple as a result of the representation of vitality compression in a small number of wavelet coefficients. Additionally, the moo recurrence components highlight the irregularities in the produced picture to provide better picture approximations. According to Figure 4, the low recurrence is the most appropriate for localizing variations in picture substance.

Jilin Daxue Xuebao (Gongxueban)/Journal of Jilin University (Engineering and Technology Edition)
ISSN：1671-5497
E-Publication Online Open Access
Vol: 41 Issue: 12-2022
DOI 10.17605/OSF.IO/MVWDU

With the aid of the low-pass and high-pass channels, the picture may be analyzed in recurrence space thanks to the depiction of wavelet change in the picture grafting location. Since tall recurrence is a far better method to show corners, edges, and lines than tall differentiation, grafting fraud creates tall differentiation in these areas. With the aid of regional clarity and elegance in the recurrence coefficients, the wavelet change characterizes these movements. To define the alterations brought on by grafting, each CC of a certain image is classified into four recurring groups (LL, HH, LH, and HL) based on these concerns (see Figure 5).

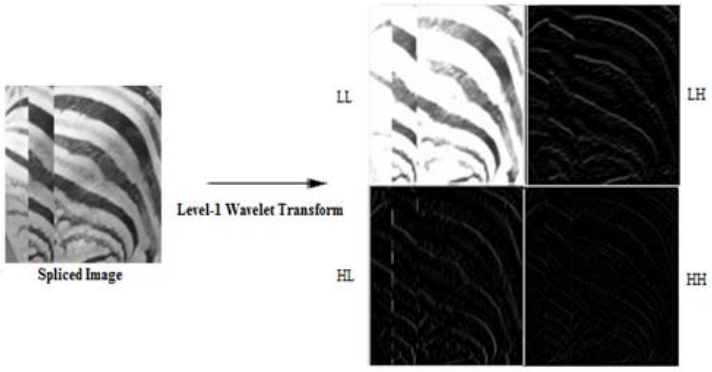

Figure 4: Disintegration of a given image into HH, LH, LL, and HL sub-bands using solo level 2D DWT.

3.2. DRLBP Histograms

The next step is to remove the distinct designs from the test image and evaluate their dispersion once the chroma channels have been removed. Because of this, we get the DRLBP signifier, which separates the HSG of neighborhood twofold designs like corners, lines, spots, and edges from the context of LBP codes [32]. Then, while taking into account the size of the nearby slope in adjacent areas, it was estimated how these designs would be implemented. DRLBP descriptor emphasizes local changes while taking the total amount of change into account. While the detailed representation of DRLBP is shown in [17], the schematic of the DRLBP descriptor is provided in conditions 1 through 4. The test image's double designs are computed from a 3x3 window with eight neighbors, after which each location's weighted histogram of double designs is computed following equation 4.

$$W_{LBP}(i) = \sum_{m=0}^{S-1} \sum_{n=0}^{T-1} G_{m,n}\, \delta\left(LBP_{m,n}, i\right) \tag{1}$$

$$\delta(j,i) = \begin{cases} 1, & j = i \\ 0, & 0 \ otherwise \end{cases} \tag{2}$$

Jilin Daxue Xuebao (Gongxueban)/Journal of Jilin University (Engineering and Technology Edition)
ISSN：1671-5497
E-Publication Online Open Access
Vol: 41 Issue: 12-2022
DOI 10.17605/OSF.IO/MVWDU

Now, n =28 is the number of canisters used to talk to the test image inside 256 distinct histograms. Indicating the commitment of the comparing twofold design regarding the focus of pixel shrewd neighboring alter is the angle greatness of the central pixel (x,y), G (x,y). ST refers to the identification of each specific recurrence band. We constructed the weighted histogram W RLBP as follows to eliminate the turnaround influence both in the foundation and frontal area:

$$WRLBP(i) = WLBP(i) + (2^8 - 1 - i), 0 \leq i \leq 2^7 \quad (3)$$

After calculating the RLBP, a computer was used to improve the discriminatory effect of double designs by computing the HSG of weighted discriminatory LBP as follows:

$$WDLBP(i) = |WLBP(i) - WLBP(2^8 - 1 - i)|, 0 \leq i \leq 2^7 \quad (4)$$

Finally, the biased RLBP and biased DLBP histograms of every neighborhood location are concatenated to create the DRLBP descriptor, which is calculated as follows:

$$DRLBP = [W_{RLBP}, W_{DLBP}]$$

3.3. Computation of DWT-DRLBP Signifier

The HOG of all sub-bands are jointed to create the DRLBP signifier after calculating the nearest descriptor $\boldsymbol{fv}$ DRLBP designs of every channel $\boldsymbol{Ch} \in \{\boldsymbol{Cb}, \boldsymbol{Cr}\}$ from all sub-bands, $\boldsymbol{sb} \in \{\boldsymbol{LL}, \boldsymbol{LH}, \boldsymbol{HL}, \boldsymbol{HH}\}$. Figure 5 depicts the entire computation of $\boldsymbol{fv}$ and explains the Calculation:

The descriptor $\boldsymbol{fv}$ calculates the majority of auxiliary changes without taking the spatial context of the image content into account. The discriminative potential of $\boldsymbol{fv}$ assist is enhanced by the incorporation of discriminative data and localized spatial changes. For this determination, every channel of the test image is divided into $\boldsymbol{S}$ blocks (sub-blocks), $\boldsymbol{B_1}, \boldsymbol{B_2}, \ldots, \boldsymbol{B_K}$, each sub-block with $\boldsymbol{s \times t}$ dimension such that $\boldsymbol{S(s \times t) = S \times T}$.The descriptor $\boldsymbol{fv\ B_i}$of each sub-block, Bi is processed. In the end the $\boldsymbol{fv\ B_i}$ of all sub-blocks is jointed correspond to the $\boldsymbol{fv^{Ch}}$ of a channel with sense to every sub-band $\boldsymbol{Sb} \in \{\boldsymbol{LL}, \boldsymbol{LH}, \boldsymbol{HL}, \boldsymbol{HH}\}$ as embodied in Equation 6. Finally, the DWT-DRLBP signifier is achieved to represent the test image as explained in Equation 5.

$$fv^{ch} = [fv^{LL}, fv^{LH}, fv^{HL}, fv^{HH}] \quad (5)$$

$$fv = [fv^{cb}, fv^{cr}] \quad (6)$$

3.4. Performance Measure and Evaluation Approach

Three photo datasets were used to evaluate the effectiveness of the suggested picture imitation localization approach. This part shows the datasets and execution assessment methodologies.

Jilin Daxue Xuebao (Gongxueban)/Journal of Jilin University (Engineering and Technology Edition)
ISSN：1671-5497
E-Publication Online Open Access
Vol: 41 Issue: 12-2022
DOI 10.17605/OSF.IO/MVWDU

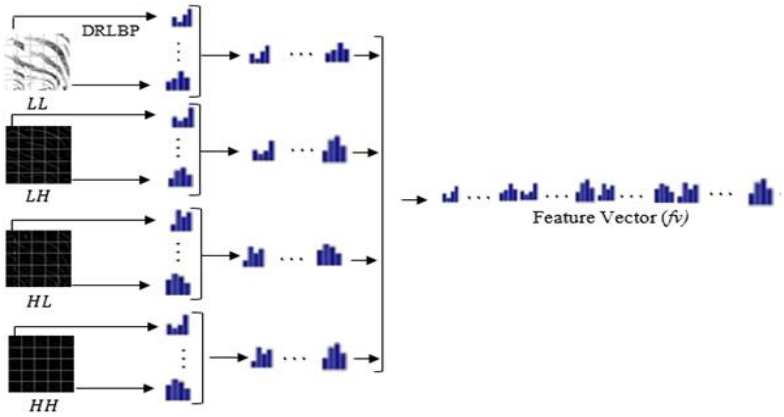

Figure 5: Encoding of spatially restricted changes happened due to splicing spending DWT-DRLBP descriptor.

Algorithm 1: Computation of DWT-DRLBP

1. RGB image I, the digit O of blocks, Switch I to YCbCr, DWT_DRLBP signifier fv
2. for every channel $Ch \in \{Cr, Cb\}$ of image I
    a) Apply 2D-DWT on Ch, Sb ∈ [HL, HH, LL, LH]
3. $Sb = HH$
4. Split Sb into O blocks: $B_1, B_2, \ldots, B_K$
5. for each block $B_o, O = 1, 2, \ldots, O$
6. Compute the DRLBP histogram fv_k^{sb}
7. $fv^{Sb} = [fv_1^{Sb}, fv_2^{Sb}, \ldots, fv_o^{Sb}]$
8. $fv^{Ch} = [fv^{LL}, fv^{LH}, fv^{HL}, fv^{HH}$
9. $fv = [fv^{Cb}, fv^{Cr}]$

3.5. Dataset Description

Utilizing three publicly existing benchmark datasets— CC (Columbia Color) DVMM [11], CASIA (1.0)[12], and CASIA(2.0)[23]—the effectiveness of the image imitation approach was evaluated. First, we ran research on DVMM to estimate the suggested tactic. Then, encourage testing and evaluations using the CASIA (1.0) and CASIA (2.0) datasets. DVMM dataset includes 180 changed images and 183 genuine images in TIFF format. The CASIA (1.0) dataset consists of 921 grafted images and 800 genuine images. Every edited image is post-processed with unique geometric adjustments. There are

Jilin Daxue Xuebao (Gongxueban)/Journal of Jilin University (Engineering and Technology Edition)
ISSN：1671-5497
E-Publication Online Open Access
Vol: 41 Issue: 12-2022
DOI 10.17605/OSF.IO/MVWDU

5,123 manufactured images and 7,491 real images in the CASIA (2.0) collection. To test the generalizability of the suggested picture imitation location strategy, we further evaluated the proposed procedure's performance on the combined dataset (a group of the 3 datasets mentioned above).

3.6. Evaluation Policy

SVM's parameters were adjusted in light of the prepared dataset. With RBF bit, we achieved the best execution. Regularized coefficient and gamma serve as two additional parameters on which the RBF channel depends. The perfect mix of these two characteristics determines how well the RBF channel will operate. By achieving the highest level of imitation location precision, the regularized coefficient plays a critical role in altering the complexity of the performance. Even though the RBF component employs the gamma parameter to describe the nonlinear mapping among two focuses, in cases when the gamma value is low, the distant missing focuses are regarded as the nearest focuses. We set the RBF bit with 25 and 2-5 for regularized constant and gamma independently applying a grid-search approach for the image grafting site [26, 27]. By randomly dividing the manufactured and authentic photographs into 10 folds of break even with an estimate, we used 10-fold cross approval. Ten execution degree values are calculated in comparison to 10-folds, and their standard deviation (std) is given as the framework's execution. For each dataset, the same approach is used again. For assessment purposes, real photographs are regarded as a negative course, whereas generated photographs are regarded as a positive course. We adopted the exactness, affectability, specificity, and erroneous positive rate evaluation tactics after taking action after execution.

Precision is the percentage of tests that are accurately predicted to be produced or true to the entire amount of test images, calculated as follows:

$$ACC = \frac{(TP + TN)}{TP + TN + FN + FP} \times 100\%. \quad (7)$$

Here, the picture TP represents the number of tests that are created, and the classifier is furthermore foreseen as being created. The image TN refers to the percentage of real photos that the classifier has also assumed to be genuine. In addition, the images FN and FP indicate the proportion of manufactured images that the classifier believes to be genuine versus the proportion of manufactured images that it believes to be true.

True progressive rate, also identified as affectability, refers to the rate of anticipating a fashioned picture as determined by the following formula:

$$TPR = SN = \frac{TP}{TP + FN} \times 100. \quad (8)$$

A genuine negative rate, also recognized as specificity, refers to the rate of assuming an honest-to-goodness picture to be just that. It is calculated as follows:

Jilin Daxue Xuebao (Gongxueban)/Journal of Jilin University (Engineering and Technology Edition)
ISSN：1671-5497
E-Publication Online Open Access
Vol: 41 Issue: 12-2022
DOI 10.17605/OSF.IO/MVWDU

$$TNR = SP = \frac{TN}{TN + FP} \times 100. \quad (9)$$

The erroneous positive rate refers to how often test images that are falsely identified as genuine are predicted to be created.

$$FPR = (1 - TNR) \times 100\%. \quad (10)$$

3.7. Parameter Tuning

The suggested framework has several parameters. The participating parameters are shown in Figure 5. It's not an easy task to tune the limitations in a thorough approach to realize the optimal set, which is why it's considered to be an optimization challenge. From a practical standpoint, parameter setup is essential. In this article, we chose several parameter settings by observation. Following parameter tweaking, Table 1 displays the key parameter values used by the suggested technique.

Table 1: The optimal limitations set of the intended technique.

Pre-processing	**Color Channel/s**	**Cb & Cr**
	Block division	**Non-overlapped**
DRLBP	P	8
	R	1
	Mapping type	u2
Classification	SVM kernel	RBF

4. RESULTS AND DISCUSSION

Table 2 demonstrates how the suggested technique performed when applied to several benchmark datasets. Figure 6 shows the appearance of the ROC bends. We connected the suggested method to the DVMM dataset to evaluate the success of the photo-grafting practices developed in this investigation. 180 regular photos and 183 styled color photographs may be found in the DVMM dataset. The produced images are created by concerning the crop-paste technique of the vertical and even strips to real photographs. Figure 6 shows the ROC bending on the datasets for the combined, DVMM (beat cleaned out), CASIA v2.0 (foot cleared out), and CASIA v1.0 (beat right) (foot right)

Table 2: Results of SVM model for image splicing detection

Dataset used	ACC	TPR	FPR	AUC
DVMM	97.32	97.69	3.80	0.96
CASIA (v1.0)	98.48	99.23	1.26	0.97
CASIA (v2.0)	98.24	97.23	0.96	0.99
Collective	98.86	99.62	2.05	0.97

Jilin Daxue Xuebao (Gongxueban)/Journal of Jilin University (Engineering and Technology Edition)
ISSN：1671-5497
E-Publication Online Open Access
Vol: 41 Issue: 12-2022
DOI 10.17605/OSF.IO/MVWDU

4.1. Robustness on Geometric Transformations

On grafted districts, geometric alterations including scaling (resizing), turn, and misshape are frequently connected in combination or in-person to mask the signs of fraud. In the CASIA(1.0) and CASIA(2.0) datasets, these alterations are linked to the grafted region(s). The accuracy of the technique against these changes is shown in Figure 6. Geometric alterations along the border create sharp edges (grafting artifacts) when connected on a joined region(s), which must be accurately described. Since grafting artifacts are genuinely captured by the DWT-DRLBP descriptor, the technique generally performs well in terms of distinctive geometric change.

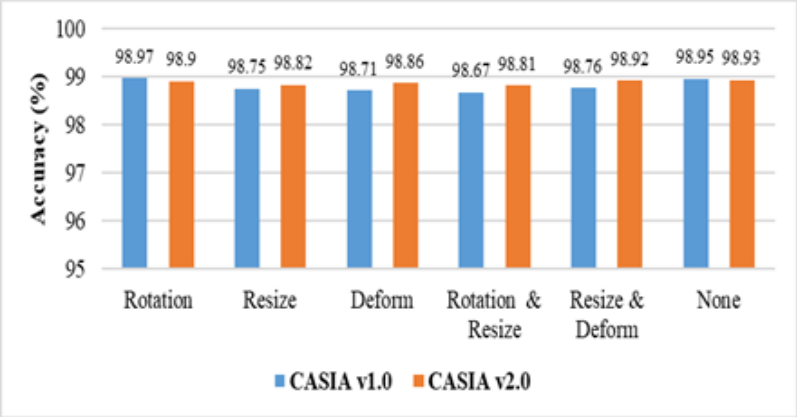

Figure 6: The proposed method accuracy on geometric transformations

Investigating different inborn features, which are often constant in untouched images, allows one to identify joining districts. The approach is examined in the small, medium, and large joined regions (s). With these sizes, Figure 8 looks to be what results. It is a proven fact that local anomalies in the linked region(s) are effective in detecting imitation, which is efficiently detected using the DTW-DRLBP signifier.

Grafting of various types of forms is very popular to obtain illegal benefits. This section looks into how connected locale shapes affect execution. The four location forms of the linked part(s), which are rectangular, subjective, triangular, and circular are contained in the CASIA (1.0) and (2.0) datasets (ARB). These shapes appear in Figure 8 as the result. The tactic works well with a variety of grafted area shapes (s).

Jilin Daxue Xuebao (Gongxueban)/Journal of Jilin University (Engineering and Technology Edition)
ISSN：1671-5497
E-Publication Online Open Access
Vol: 41 Issue: 12-2022
DOI 10.17605/OSF.IO/MVWDU

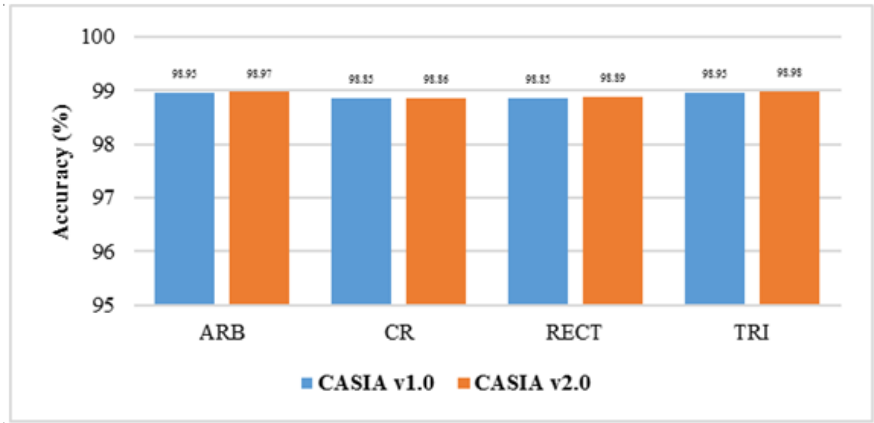

Fig 7: The intended method precision on spliced region(s) shape.

The suggested procedure's execution was evaluated using JPEG images from the CASIA (1.0) and (2.0) datasets, and it achieved 98.1% accuracy. DCT quantization is used to achieve JPEG compression. The fraud that occurs when grafting is done in JPEG images takes the form of piece jumbling and squares that are not adjusted with their neighbors, leading to unnecessary edges. Because the DWT-DRLBP descriptor was used to properly explore the irregularities within the combined picture, the suggested strategies achieved high imitation discovery precision.

In this portion, we evaluated the results of this investigation of the most recent photo grafting technique for image imitation. Since they attained the best consequences both on CASIA (1.0), CASIA (2.0), or DVMM, Table 3 shows the execution of cutting-edge methods as it were on the contrasting datasets. It demonstrates how, in terms of each execution assessment criterion, the suggested technique outperformed the most recent methodologies. Additionally, it should be noted that the applicability of the suggested technique was made possible by the fact that the proposed approach worked effectively on mixed datasets.

Table 3: Difference with the latest state-of-the-art image splicing detection techniques

Approaches	Dataset used	ACC	TPR	FPR	AUC
Proposed	CASIA v (1.0)	98.48	99.23	1.26	0.97
	DVMM	97.32	97.69	3.80	0.96
	CASIA v (2.0)	98.24	97.23	0.96	0.99
	All	98.86	99.62	2.05	0.97
[5]	CASIA v (1.0)	94.68	92.22	2.77	0.92
	DVMM	96.28	97.61	4.46	0.99
	CASIA v (2.0)	97.14	98.41	3.47	0.96
[28]	CASIA v (1.0)	96.28	97.56	6.84	–
	DVMM	91.23	93.18	16.14	–
	CASIA v (2.0)	97.57	98.73	2.74	–
[6]	CASIA v (2.0)	96.12	92.89	2.92	-
	CASIA v (1.0)	90.29	92.79	2.11	-
	Both	94.55	92.59	7.22	-

Jilin Daxue Xuebao (Gongxueban)/Journal of Jilin University (Engineering and Technology Edition)
ISSN：1671-5497
E-Publication Online Open Access
Vol: 41 Issue: 12-2022
DOI 10.17605/OSF.IO/MVWDU

In comparison to other cutting-edge strategies, the strategy maintains a low untrue positive rate while having high exactness and genuine positive rates overall.

5. CONCLUSION

We used the DWT-DRLBP signifier for inclusion extraction to talk to a test image for verification. To take advantage of grafting inconsistencies, chroma modules of a sample image are degraded into sub-bands applying solo-level DWT. To capture the detailed insights from these sub-bands, a powerful surface descriptor called DRLBP is used. The suggested technique is capable of identifying joining picture imitation in fact when post-processing procedures are imminent thanks to the DWT-DRLBP descriptor. DWT-DRLBP signifier execution is found and examined using an SVM classifier along with a 10-fold cross-approval. The tests and evaluations used three freely available benchmark datasets. Our suggested strategy is strong when matched to other state-of-the-art strategies and achieved 98.94% exactness on the joint dataset. These outcomes moreover bolstered the effectiveness of the DWT-DRLBP descriptor, which was utilized to show distortions in images brought by joining imitation. Additionally, SVM with RBF classified each given image as genuine or joined, and finally assured the astounding precision of outcomes. Long-term efforts are being made to localize the joined region(s) to increase belief in outcomes and to level the degree of joining.

References

1. Khurshid A, Zulfiqar H, Muhammad H. Copy-move and splicing image forgery detection and localization techniques: a review. Australian Journal of Forensic Sciences 2017;*49:*281-307.
2. Zhao X, Li J, Li S, Wang S. Detecting digital image splicing in chroma spaces. In Proceedings of International workshop on digital watermarking, Berlin, Germany 2010:12-22.
3. Xunyu P. Digital image forensics with statistical analysis. Handbook of digital forensics of multimedia data and devices. John Wiley & Sons; 2015. 481 p.
4. Mahmoud E, Hongli Z. Two-stage keypoint detection scheme for region duplication forgery detection in digital images. J Forensic Sciences 2017;63:102-11.
5. Muhammad, G, Al-Hammadi M, Hussain, M, Bebis G. Image forgery detection using steerable pyramid transform and local binary pattern. Machine Vision and Applications 2014;25:985-995.
6. Goh J, Thing VL, A hybrid evolutionary algorithm for feature and ensemble selection in image tampering detection. International Journal of Electronic Security and Digital Forensics 2015;7:76-104.
7. Alahmadi AA, Hussain M, Aboalsamh H, Muhammad G, Bebis G. Splicing image forgery detection based on DCT and Local Binary Pattern. In Proceedings of IEEE Global Conference on Signal and Information Processing, Austin, TX, USA 2013:253-256.
8. Min GH, Dong HH. Identification method for digital image forgery and filtering region through interpolation. J Forensic Sciences 2014;59:1372-1385.
9. Jinwei W, Qiye N, Guangjie L, Xiangyang L, Sunil KJ. Image splicing detection based on convolutional neural network with weight combination strategy. J Information Security and Applications 2020;54:1-8.

ISSN：1671-5497
E-Publication Online Open Access
Vol: 41 Issue: 12-2022
DOI 10.17605/OSF.IO/MVWDU

10. Costanzo A, Amerini I, Caldelli R, Barni M. Forensic analysis of SIFT keypoint removal and injection. IEEE Transactions on Information Processing and Security 2014;9:1450-1464.
11. Ng TT, Chang SF, Sun Q. A data set of authentic and spliced image blocks, Columbia University 2004:6-9.
12. Dong J, Wang W. CASIA image tampering detection evaluation databases. In Proceedings of Signal and Information Processing 2015, Beijing, China:422-426.
13. Ng TT, Chang S.F, Sun Q, Blind detection of photomontage using higher order statistics. In Proceedings of international symposium on circuits and systems 2004, Vancouver, Canada:688-691.
14. Hsu F, Chang S, Detecting image splicing using geometry invariants and camera characteristics consistency. In Proceedings of IEEE International Conference on Multimedia and Expo 2006, Seattle,USA: 549-552.
15. Shi YQ, Chen C, Chen W. A natural image model approach to splicing detection. In Proceedings of 9th ACM Workshop on Multimedia & Security Proceedings 2007, Dallas, Texas:51-62.
16. Wang W, Dong J, Tan T, Image tampering detection based on stationary distribution of Markov Chain. In Proceedings of 17th IEEE international conference on image processing 2010, Hong Kong:2101-2104.
17. Zhao X, Li S, Wang S, Li J, Yang K. Optimal chroma-like channel design for passive color image splicing detection. EURASIP Journal on Advances in Signal Processing 2012;2012:1-11.
18. Park TH, Han JG, Moon YH, Eom IK, Image splicing detection based on inter-scale 2D joint characteristic function moments in wavelet domain. EURASIP Journal on Image and Video Processing 2016;2016:30-39.
19. Alahmadi A, Hussain M, Aboalsamh H, Muhammad G, Bebis G, Mathkour H, Passive detection of image forgery using DCT and local binary pattern. Signal, Image and Video Processing 2017;11:81-88.
20. Pham NT, Lee JW, Kwon GR, Park CS. Efficient image splicing detection algorithm based on markov features. Multimedia Tools and Applications 2018: 1-15.
21. Jalab HA, Subramaniam T, Ibrahim RW, Kahtan H, Noor NFM. New texture descriptor based on modified fractional entropy for digital image splicing forgery detection. Entropy 2019; 21:371-385.
22. Gonzalez RC, Woods RE. Digital image processing. Addison-Wesley Reading: 1992; 4.
23. Satpathy A, Jiang X, Eng HL. LBP-based edge-texture features for object recognition. IEEE Transactions on Image Processing 2014;23:1953-1964.
24. Cortes C, Vapnik V, Support-vector networks. Machine Learning 1995;20:273-297.
25. Chang CC, Lin CJ. LIBSVM: a library for support vector machines. ACM Transactions on Intelligent Systems and Technology 2011;27:21-27.
26. Hsu CW, Chang CC, Lin CJ. A practical guide to support vector classification. 2003.
27. Sokolova M, Japkowicz N, Szpakowicz S. Beyond accuracy, F-score and ROC: a family of discriminant measures for performance evaluation. In Proceedings of Australasian joint conference on artificial intelligence, Berlin, Germany 2006:1015-1021.
28. Agarwal S, Chand S. Image forgery detection using multi scale entropy filter and local phase quantization. I J Image, Graphics and Signal Processing 2015;10:78-85.
29. Chen J, Kang X, Liu Y, Wang ZJ. Median filtering forensics based on convolutional neural networks. IEE Signal Processing Letters 2015;22:1849-1853.

ISSN：1671-5497
E-Publication Online Open Access
Vol: 41 Issue: 12-2022
DOI 10.17605/OSF.IO/MVWDU

30. Zhao X, Wang S, Li S, Li J. Passive image-splicing detection by a 2-D noncausal Markov model. IEEE Transactions on Circuits and Systems for Video Technology 2015;25:185-199.
31. Hussain M, Qasem S, Bebis G, Muhammad G, Aboalsamh H, Mathkour H. Evaluation of image forgery detection using multi-scale weber local descriptors. International Journal on Artificial Intelligence Tools 2015;24:1-28.
32. Akram A, Ramzan S, Rasool A, Jaffar A, Furqan U, Javed W. Image splicing detection using discriminative robust local binary pattern and support vector machine. World Journal of Engineering. 2022 Feb 14.